Experimental investigation of excited states in atomic dysprosium

Dmitry Budker, David DeMille, and Eugene D. Commins
Physics Department, University of California, Berkeley, Berkeley, California 94720

Max S. Zolotorev
Stanford Linear Accelerator Center, Stanford, California 94309
(Received 7 April 1993; revised manuscript received 17 February 1994)

A pair of closely lying states of opposite parity and the same total electronic angular momentum ($J=10$) at 19797.96 cm^{-1} in dysprosium is experimentally investigated with the goal of evaluating parameters relevant to parity and parity–time-reversal violation experiments. An atomic beam apparatus is used. The states of interest are populated with a sequence of two laser pulses, and a third laser pulse and fluorescence detection are used to probe the state population. Their lifetimes are determined from the dependence of the fluorescence signal on the time delay between the pump and probe pulses. The lifetime of the even-parity state was also measured by a different method involving detection of cascade fluorescence. Spectroscopy of radio-frequency $E1$ transitions between the opposite-parity states is performed when one of the states is populated and the population of the other is probed. This determines precise energy separations between various isotope and hyperfine structure components, and allows extraction of the corresponding isotope shift and hyperfine structure parameters. Electric polarizability is determined from radio-frequency line shapes in the presence of a dc electric field. As part of the preparation of a parity violation experiment, level-crossing signals which occur when various Zeeman components of the closest hyperfine components (isotope 163, $F=10.5$; initial separation 3.1 MHz) are brought together in the presence of collinear electric and magnetic fields were studied. These measurements provide an independent determination of the $E1$ matrix element between the opposite-parity states. In addition, lifetimes, isotope, and hyperfine structure of other dysprosium states are obtained and a number of narrow autoionization resonances ($\Gamma < 10$ cm^{-1}) are observed.

PACS number(s): 35.10.−d, 32.30.−r, 32.60.+i, 32.70.−n

I. INTRODUCTION: PARITY AND TIME-REVERSAL INVARIANCE VIOLATION EXPERIMENTS IN DYSPROSIUM

Violation of discrete space-time symmetries in atoms and molecules has been a subject of intense experimental and theoretical research for the last several decades. This research has concentrated mainly in two principal directions: the search for permanent electric dipole moments (EDM's), which can arise only if both parity (P) and time reversal (T) invariance are violated; and measurement of parity nonconservation (PNC) effects such as natural optical activity of an atomic vapor and PNC-Stark interference (for recent reviews of the field see, e.g., [1–4]). Although atomic experiments on P and P,T violation have already provided important results such as, e.g., quantitative tests of the Standard Model of the electroweak interactions and the most stringent limit on the electron EDM, it is still important to improve experimental sensitivity. In the case of EDM's, it is very desirable to observe an atomic T-odd effect or set better limits on it in the absence of a satisfactory theory to explain the only known case of CP (C denotes charge conjugation) violation in the decay of neutral kaons [5]. In the case of PNC, one seeks to uncover relatively small but important effects such as differences of PNC amplitudes for different isotope and hyperfine components of a given transition. The former provides a test of the standard model of the electroweak interactions and possible extensions to it [1], while the latter, in addition to the nuclear spin-dependent part of the electron-nucleus interaction, has a contribution from the so-called anapole moment ([6] and references therein), which arises due to weak interactions among nucleons. Therefore, one is interested in finding systems that are suitable for these experiments and which offer maximum enhancement of the effects under consideration.

In atomic dysprosium (Dy) there exists a pair of nearly degenerate states of opposite parity and the same angular momentum ($E=19797.96$ cm^{-1}, $J=10$; levels A and B, Fig. 1). These states are of interest for parity and time-reversal experiments [8] because P- and P,T-odd effects are enhanced by the extremely small energy separation. Since $Z=66$ for Dy, the well-known enhancement [9,6] approximately proportional to Z^3 is also present. Additional advantages may arise from the fact that A and B are expected to have relatively long lifetimes from an analysis of possible fluorescence decay channels. On the other hand, various dilutions and cancellations in the expected P- and P,T-odd effects exist due to the complexity of the multielectron configurations involved. Moreover, in the case of PNC, the dominant configurations of A and B are not mixed by the weak interaction; the effect arises only from configuration mixing and core polarization [10]. Thus, to design practical P and P,T experiments, one must obtain detailed spectroscopic information about these near-degenerate states.

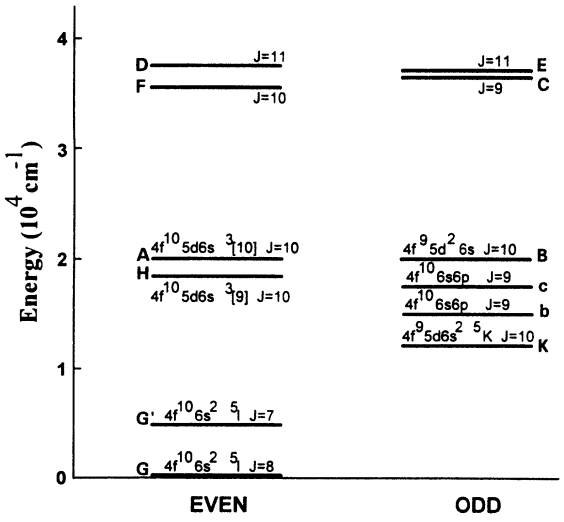

FIG. 1. Partial energy level scheme in atomic dysprosium. The level energies (in cm^{-1}) are: A,B—19797.96, b—15972.35, c—17727.15, C—36341.53, D—37299.36, E—37182.98, F—35385.78, G'—4134.23, H—18462.65, K—12892.76. For a compilation of energy levels, momenta, configurations and g values, see [7].

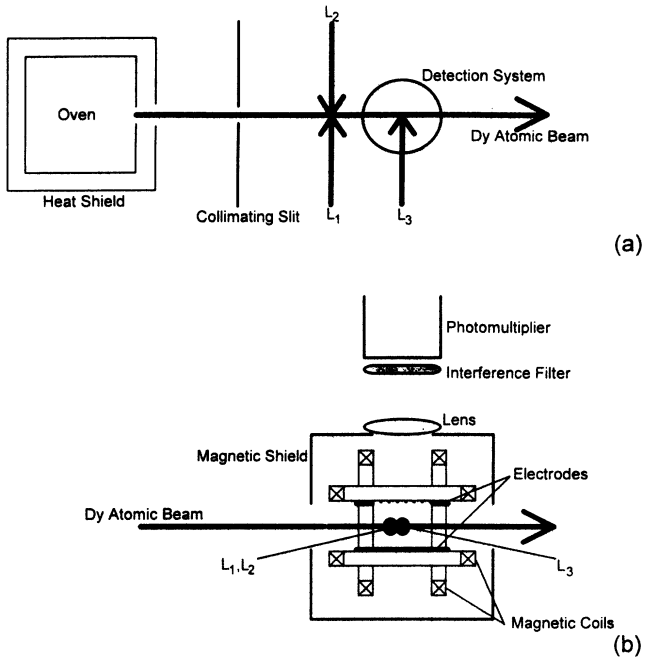

FIG. 2. Schematic of the apparatus. (a) top view; for the lifetime measurements (Sec. III), the pump laser beams $L_{1,2}$ were spatially separated from the probe beam L_3, electrodes and magnetic shield were not used. (b) side view of the interaction region in the configuration used for rf measurements (Secs. IV,VII).

In the present research, practical schemes were realized for state population and detection utilizing consecutive laser-induced transitions and fluorescence detection. The lifetimes of states A and B, the $E1$ matrix element between these states, and isotope shift and hyperfine structure parameters were measured. The results obtained give solid grounds for designing P- and P,T-violation experiments and will facilitate ongoing theoretical calculations of the corresponding effects in Dy [10]. A brief initial report of parts of this work was given in [11].

II. METHODS OF STATE PREPARATION AND DETECTION

The experiment utilized an apparatus [12] schematically shown in Fig. 2. The dysprosium beam was produced in an effusive source which incorporated a tantalum oven resistively heated with tantalum wire heaters to ~1550 K (corresponding to a vapor pressure of ~0.1 Torr). Dysprosium with natural isotopic abundance was used (156:0.05%; 158:0.09%; 160:2.29%; 161:18.88%; 162:25.53%; 163:24.94%; 164:28.18%). Isotopes 161 and 163 both have nuclear spin $I=\frac{5}{2}$. Neither of the states of interest ($J=10$) is connected to the ground state ($J=8$) by a dipole transition; therefore, they were populated by using two consecutive transitions induced by pulsed dye lasers.[1] Several different combinations of transitions were used. In the population schemes used originally [11], the first pulse excited the atoms from the ground state to a high-lying state, while the second induced stimulated emission to bring the atoms to the state of interest. In

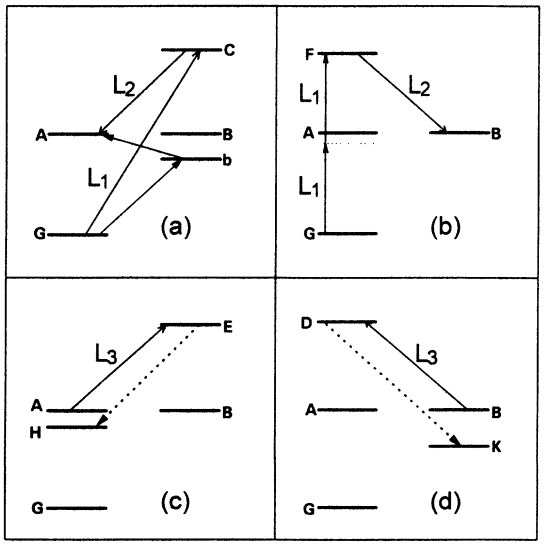

FIG. 3. Population and probe schemes for the states A and B. Solid lines, laser-induced transitions; dashed lines, selectively detected fluorescence channels. Level designation corresponds to Fig. 1.

[1]The $E2$ transition from the ground state to the even parity state is expected to be suppressed because the total spin is different for the two levels. For the same reason, in the stepwise $E1$-$E1$ excitation schemes at least one of the $E1$ transitions is expected to be suppressed, and this is indeed observed experimentally.

the case of the even parity state (A) these were two $E1$ transitions [GC and CA, Fig. 3(a)], and in the case of the odd state (B) these were a two photon and an $E1$ transition [GF and FB, Fig. 3(b)]. The dye lasers were Quanta Ray PDL-1 and PDL-2 (pumped with a Quanta Ray DCR-2 Nd-YAG laser), operated in a broadband mode (without intracavity etalons) with typical line width 0.5 cm^{-1}. In order to produce 275-nm photons necessary to excite the GC transition [Fig. 3(a)], the output frequency of one laser was doubled with a KD*P crystal. The two population pulses were spatially superimposed with each other in the region where they intersected the atomic beam and were temporally separated by several nanoseconds, so that the intermediate state population did not decay significantly due to spontaneous emission between the population pulses (see Sec. IX: Auxiliary Lifetime Measurements). Typical pulse energies were ~ 1 mJ, duration ~ 7 ns, repetition rate 10 Hz. In the interaction region ~ 10 cm downstream from the oven, the laser beam diameters were ~ 3 mm and the atomic beam density $\sim 5\times 10^9$ atoms/cm^3.

It was found, however, that both these schemes have a common drawback related to the fact that the first stages of these schemes involve transitions which require relatively high laser power (the 275-nm $E1$ transition is strongly suppressed). As a result, there is a high probability for an atom excited to the upper state of the transition to absorb an additional photon and ionize. In order to avoid this, a different population scheme for the state A was used in later experiments [Fig. 3(a), transitions Gb and bA]. In this scheme, light at 626 nm for the transition Gb was generated with a dye laser, while the 2614-nm infrared radiation for the bA transition was produced by nonlinear mixing (in a 35-mm-long $MgO:LiNbO_3$ crystal) of a part of the output of the same laser and the light from the other dye laser operating at 823 nm. With typical pulse energies 3 mJ at 626 nm and 8 mJ at 823 nm at the crystal, up to 0.1 mJ of the 2614-nm radiation was obtained.

In order to detect the population of state A or B, a third (probe) laser pulse was used to excite an $E1$ transition from this state [transitions AE and BD, Figs. 3(c) and 3(d)], and fluorescence from the upper state of this transition was detected. The probe pulses were generated with a pulsed dye amplifier [13] seeded with a cw dye laser and pumped with another DCR-2 Nd-YAG laser. The pulse energy, duration and beam size for the probe beam were similar to those of the pump beams. The pulsed dye amplifier output has a nearly Fourier-transform-limited bandwidth ~ 150 MHz. However, pulse energies ~ 1 mJ were sufficiently large so that all isotope and hyperfine components were excited when the frequency was tuned close to resonance. In order to perform spectroscopy on a probe transition (Sec. VIII), the probe beam was attenuated by a factor ~ 20; at this reduced pulse energy all the components were resolved. The fluorescence detection system consisted of a lens, an interference filter to select a desired fluorescence channel and a photomultiplier (Burle 8850). The laser-pulse timing and data acquisition were controlled through CAMAC electronics.

III. LIFETIME MEASUREMENTS OF THE STATES A AND B

In the early work reported in [11], in order to determine the lifetimes of states A and B, the state under investigation was populated and its population was probed after a time delay. The probe laser beam intersected the atomic beam downstream from the pump region [see Fig. 2(a)]. Typical separations between the pump and the probe regions were 1–5 cm. With fixed spatial separation, the fluorescence signal was recorded as a function of time delay between the pump and probe pulses, while this delay was varied in the range 5–60 μs for state A and 10–400 μs for state B. An example of this data is shown in Fig. 4(a).

For pump and probe regions of length dL separated by distance L, and assuming a modified Maxwellian velocity distribution for the atomic beam [14], one expects the fluorescence signal S to depend on the time delay t according to

$$S=\alpha\left[\frac{L^2}{t^2}\right]\exp\left[-\left[\frac{L}{V_0 t}\right]^2-\frac{t}{\tau}\right]\frac{dL}{t}+\beta\,, \tag{1}$$

where $V_0=(2kT/M)^{1/2}$, τ is the lifetime of the state of interest, α is a scale constant and β is an overall background due to electronics, small amount of scattered probe laser light, etc. The experimental results were fitted to this formula integrated over the finite size of the pump and probe regions dL, and a χ^2-minimization procedure [15] was used to determine free parameters in the fit: α, β, τ, and T. For each of the states A and B and for various values of the separation L, these fits gave consistent results for the lifetimes and the values of T close to the actual oven temperature. The combined extracted lifetime values were: $\tau(A)=8(1)$ μs and $\tau(B)=130(30)$ μs (with uncertainties corresponding to 68% C.L.). This method of long lifetime measurement has the advantages that the laser beams are spatially fixed, that it is insensitive to inhomogeneities of the fluorescence detection system (the fluorescent light always comes from the same place) and no assumptions have to be made about the exact geometry of the atomic beam, spatial overlap between the atomic and laser beams, etc. However, this method is subject to certain systematic effects, particularly for the longer lifetime state B. For example, it depends on the knowledge of the velocity distribution in the atomic beam and deviations from the assumed modified Maxwellian distribution are sometimes observed in effusive beam experiments ([14] and references therein). In order to calibrate the system and make it insensitive to such systematics, the present lifetime measurements of the state B included measurements on several "control" metastable levels: the $J=7$ state in the ground state term (level G' on Fig. 1), the lowest odd parity state with $J=10$ (level K) and also the odd parity state $4f^{10}6s6p$ $J=10$ at 17 513.33 cm^{-1}. These states do not have allowed decay channels and are, therefore, expected to have very long lifetimes. Examples of data from this measurement series are shown in Fig. 4(b). It was found that within experimental uncertainties the time dependence was the same

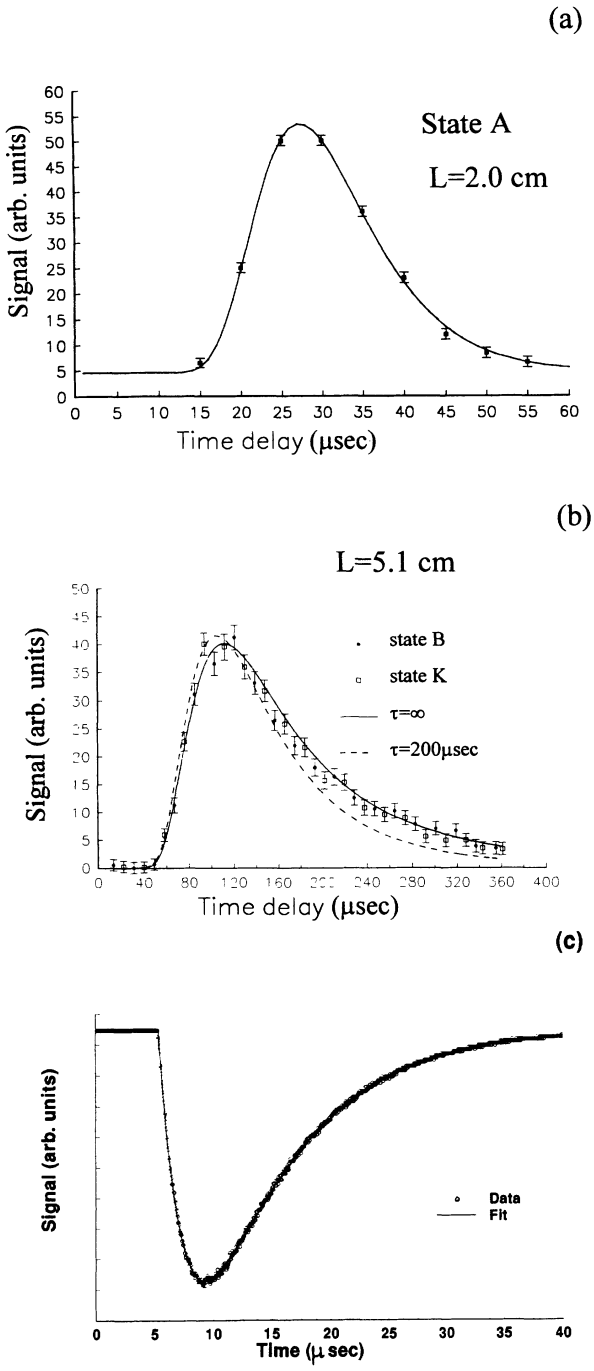

FIG. 4. (a) An example of data used to extract the lifetime of state A. The fluorescence signal (points with error bars) which is a measure of the state population was taken as a function of time delay between the pump and probe pulses with fixed spatial separation ($L=2.00$ cm, $dL=0.18$ cm) between corresponding laser beams. Solid line—a fit according to the procedure described in the text. For the shown fit, the extracted values of parameters are $\tau=7.7(7)$ μsec, $T=1550(80)$ K, $\beta=4.6(9)$ arb. units. (b) Examples of the lifetime data for the state B and a control state K. Also shown are expected signal time dependences with $\tau=\infty$ and 200 μsec and $T=1300$ K, $L=5.1$ cm, $dL=0.1$ cm. (c) Fluorescence data used for the lifetime measurement of the state A. The detection system was sensitive to the cG transition at 564 nm of the Ac,cG decay cascade. The data represents an average over 256 consecutive pulses.

for all the control levels, and also for the state B. Assuming infinite lifetime for the control levels, from the data one obtains a lower limit on the lifetime of B: $\tau_B > 200$ μsec (95% C.L.). In addition, the observed time dependences were in agreement with predictions of Eq. (1) with infinite lifetimes [see Fig. 4(b)]. The result for τ_B is in some disagreement with our previous measurement. The reason for this is not understood. However, as pointed out above, the old measurement did not include control lines and was potentially subject to systematics. It should also be noted that certain changes were introduced in the system between the two measurement series. In particular, the length and shape of the oven nozzle channel were changed so that with the same density of atoms in the interaction region the oven was operated at significantly lower temperatures. Therefore it is impossible to directly project the level of agreement of the present observations with the predictions of Eq. (1) to the old data.

The lifetime of the state A was also measured with a different method. From an analysis of possible decay channels of this state and a calculation of Kozlov, Dzuba, and Flambaum [10], it is expected that the two principal decay channels of A are by infrared transitions to the states b and c (see Fig. 1). State c decays to the ground state ($\lambda=564$ nm) and its lifetime has been measured in [16] [$\tau_c=2.15(10)$ μsec] and in [17] [$\tau_c=2.7(4)$ μsec]. If the state A is populated at $t=0$ and one observes cascade fluorescence in the 564-nm channel, the expected signal time dependence is given by

$$S \propto \frac{\tau_c}{\tau_A-\tau_c}(e^{-t/\tau_A}-e^{-t/\tau_c}) . \quad (2)$$

In order to observe this dependence, the state A was populated through the Gb,bA transition sequence [Sec. II, Fig. 3(a)]. To make the fluorescence detection system homogeneous over the fluorescence region size ~1 cm (i.e., the distance the atoms in the atomic beam travel in several lifetimes of the state A), these measurements were taken without the fluorescence collecting lens. A narrow bandpass interference filter for the 564-nm fluorescence was placed in front of the photomultiplier tube (PMT). The PMT signal was digitized and averaged over many laser pulses with a Tektronix 2430A digital oscilloscope. The data was then fit to the temporal dependence given by Eq. (2) yielding the following values of the lifetimes: $\tau_c=2.20(4)$ μsec and $\tau_A=7.9(2)$ μsec, where the uncertainties are dominated by estimated systematic effects due to the finite size of the fluorescence region. These values are in agreement with previous measurements and have smaller uncertainties. The data and the fit are shown in Fig. 4(c).

In conclusion, the final results for the lifetimes of the nearly-degenerate states are $\tau_A=7.9(2)$ μsec, $\tau_B>200$ μsec. Lifetime measurements of a number of other states in dysprosium are described in Sec. IX.

IV. RADIO-FREQUENCY ELECTRIC-DIPOLE TRANSITIONS

In order to determine energy separations between various isotope and hyperfine components of A and B, radio-

frequency (rf) electric-dipole transitions were induced between them. To do this, the pump and probe laser beams were brought close together [see Fig. 2(b)], state A was populated, and the population of state B was probed 5–10 μs later. A cw rf electric field was created in the interaction region by a pair of plane-parallel electrodes. One of the electrodes was made of a wire grid, partially transparent for fluorescence light. The influence of laboratory magnetic fields was reduced with a single 1-mm layer of annealed CO-NETIC[2] magnetic shielding (residual magnetic-field level $\sim 10^{-2}$ G). The studied rf frequency range was 200 kHz–2 GHz. Below 1 GHz, the rf frequency was generated directly by a Fluke 6060 synthesized signal generator; to obtain frequencies above 1 GHz, the output of the generator was frequency doubled with a nonlinear crystal. The rf signal was amplified with a power amplifier and connected with a 50-Ω line to the electrodes which were terminated with a power absorbing 50-Ω resistor. At frequencies ~ 1 GHz and above, plungers were used to match the electrodes to the 50-Ω line and reduce reflections back into the amplifier. The electric-field amplitude between the field plates was ~ 10–100 V/cm.

The experimental procedure consisted of scanning the radio frequency (with the lasers tuned to their corresponding resonances) and recording the fluorescence signal. A number of rf resonances were observed (Table I, column 1). Although the amplitude of the rf field between the electrodes varied with frequency and was not carefully monitored, the observed resonances could be qualitatively divided into three groups according to their intensity (under conditions when they were not saturated in rf power). The "very strong" resonances had intensity roughly a factor of five greater than the "strong" resonances, which in turn had intensity at least an order of magnitude greater than the "weak" ones. The very strong and weak resonances are marked in Table I with letters vs and w, respectively. The line shapes of the rf resonances fit well to the expected line shape which was obtained by numerical integration of the Schrödinger equation. Although the lifetime of state A is comparable to the time interval t between population and probe pulses, this line shape was similar to the line shape in the case of infinite lifetimes (see, e.g., [14]) and had typical unsaturated width $\Delta\nu = t^{-1} \sim 150$ kHz.

TABLE I. Observed rf $E1$ transitions. Very strong and weak transitions are marked in column 1 by the letters vs and w, respectively. Transition identification and frequency signs were obtained through analysis described in the text. Very strong resonances correspond to the most abundant even isotopes, weak resonances are $\Delta F = \pm 1$ transitions for odd isotopes.

ν_{rf}, MHz	Isotope	F_A	F_B
−1328.64(6)	160	10	10
−1714.70(4)	161	11.5	11.5
−1249.72(4)	161	10.5	10.5
−962.26(3) w	161	12.5	11.5
−791.47(2)	161	9.5	9.5
−349.21(2)	161	8.5	8.5
−172.66(2) w	161	11.5	10.5
68.83(3)	161	7.5	7.5
514.01(3)	161	10.5	9.5
−234.69(2) vs	162	10	10
−1581.02(3)	163	7.5	7.5
−1134.78(4)	163	8.5	8.5
−609.67(2)	163	9.5	9.5
−363.01(3) w	163	7.5	8.5
3.10(2)	163	10.5	10.5
504.68(3) w	163	8.5	9.5
713.10(2)	163	11.5	11.5
1530.87(3)	163	12.5	12.5
753.53(2) vs	164	10	10

[2]Magnetic Shield Corporation, Perfection Mica Company, 740 North Thomas Dr., Bensenville, IL.

V. INTERPRETATION OF THE OBSERVED rf TRANSITIONS

In order to interpret the observed resonances which correspond to different isotope and hyperfine components of the transition $A \rightarrow B$, the following procedure was carried out. First, information about the total angular momenta $F_{A,B}$ of the initial and final state for each transition was obtained by observing the rf line shapes in the presence of a dc magnetic field. A magnetic field ~ 0.1–0.5 G parallel or perpendicular to the rf electric field (z- and x-magnetic field, respectively) was created with pairs of Helmholz coils installed inside the magnetic shield [Fig. 2(b)]. An example of an experimental rf line shape in the z-magnetic field is shown in Fig. 5 along with calculated line shapes for $\Delta F = 0, \pm 1$ transitions. The rf line shapes (unsaturated in rf power) were calculated as sums over all Zeeman components of the two-level rf line shapes taking into account their Zeeman shifts and the

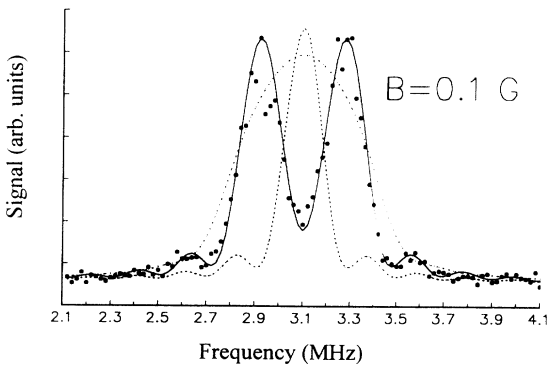

FIG. 5. Line shape of a $\Delta F = 0$ transition (isotope 163, $F_A = F_B = 10.5$) in a magnetic field parallel to the rf electric field. Circles: experimental points; averaging—10 pulses per point. Solid line: a fit with $\Delta F = 0$ line shape. This line shape is insensitive to F, but allows unambiguous determination of ΔF. Dashed and dotted lines: line shapes of a $\Delta F = 1$ and a $\Delta F = -1$ transitions, respectively (with arbitrary vertical scales).

TABLE II. Values of parameters obtained from interpretation of observed rf transitions. W: state energy (without hyperfine interactions for odd isotopes); a: magnetic-dipole interaction constant; b: electric-quadrupole interaction constant; c: effective magnetic-octupole interaction constant. Standard definitions of the hfs parameters are used (see, e.g., [14]).

Isotope	W_B-W_A, MHz	a_A, MHz	b_A, MHz	a_B, MHz	b_B, MHz	c_B-c_A, MHz
156	−4201(30)[a]					
158	−2385(15)[a]					
160	−1328.64(6)					
161	−1160.68(3)	−113.177(3)	1766.1(2)	−155.652(3)	1950.8(3)	0.005(15)
162	−234.69(2)					
163	−7.38(1)	158.52(1)	1865.0(5)	218.11(1)	2059.8(5)	−0.027(7)
164	753.53(2)					

[a]rf transitions involving isotopes 156,158 were not observed since they lie outside the studied frequency range. The values of W_B-W_A were deduced from isotope shift analysis (see text).

corresponding Clebsch-Gordan coefficients. The Lande factors g_F necessary to evaluate the Zeeman shifts were calculated from the known values $g_J(A)=1.21$ and $g_J(B)=1.367$ according to $g_F \cong g_J[F(F+1)+J(J+1)-I(I+1)]/2F(F+1)$. (The g_J values and references to original work of Conway, Worden, and Wyart are given in [7].)

The line shapes in the z-field allowed determination of $\Delta F = F_B - F_A$ for each resonance. All strong resonances were found to be $\Delta F = 0$. Indeed, one expects the intensities of $\Delta F = 0$ transitions to be greater than those of $\Delta F = \pm 1$ transitions by a factor[3] ~ 30.

For $\Delta F = 0$ transitions, the line shape in a z field is insensitive to the value of F. Therefore, in order to determine the F values for $\Delta F = 0$ transitions, rf line shapes in an x-magnetic field were studied. It was possible to determine the F values from these line shapes with a typical uncertainty ± 1 unit.

After these steps were carried out, computer sorting of hypotheses about $\Delta F = 0$ transitions (including even-isotope transitions for which $F = J$) was carried out. For $\Delta F = 0$, the energy differences depend only on the energy separation $W_B - W_A$ without hyperfine interaction, and the *differences* of hyperfine constants. In addition, we made use of the known ratios of nuclear magnetic dipole and electric quadrupole moments for the odd isotopes [18]. We also required linearity in the King plot (Sec. VI) for isotope shifts in the rf transition versus isotope shifts in optical transitions [19]. As a result of this analysis, a unique hypothesis describing the $\Delta F = 0$ transitions was found, and the following parameters were extracted (up to an overall sign): W_B-W_A, a_B-a_A, b_B-b_A, c_B-c_A. Here a, b, and c are magnetic dipole, electric quadrupole, and effective magnetic octupole hyperfine structure (hfs) constants, respectively. The remaining sign ambiguity was resolved using the isotope shift analysis of Wyart [21] and confirmed by performing spectroscopy on the probe transition (see Sec. VIII). In the latter experiment, it was also possible to measure directly several hyperfine intervals of state B with a relatively high uncertainty ~ 30 MHz. This together with the measured frequencies of the $\Delta F = \pm 1$ transitions provided more than enough information to determine the hyperfine constants for each state A,B separately. A summary of the deduced parameters is given in Table II. Using these parameters it is possible to verify that all $E1$ resonances expected in the studied rf frequency range were indeed observed.

[3]The relative intensities can be calculated in a straightforward way. They follow a rule that for the strongest transitions, $\Delta F = \Delta J$. This is analogous to fine structure multiplet components in the LS approximation where for the most intense transitions, $\Delta J = \Delta L$. For corresponding formulas and discussion see, e.g., [20].

VI. ANALYSIS OF ISOTOPE SHIFT AND HYPERFINE STRUCTURE

Differences between the values of W_B-W_A for different isotopes (Table II, column 2) constitute isotope shifts in the transition $A \rightarrow B$. We note that since this transition lies in the rf range, the precision of the present isotope shift measurement is about two orders of magnitude higher than that of typical isotope shift measurements in optical spectra [22]. In dysprosium, isotope shifts in a number of optical transitions were measured in [19]. Using one of the optical transitions as a reference ($\lambda = 563.95$ nm, $G \rightarrow 4f^{10}6s6p, {}^5K_9$), a King plot analysis [22] of the rf isotope shift was carried out. From the slope of the King line (Fig. 6), the ratio of the electronic field shift parameters $E_{A\rightarrow B}/E_{\text{ref}} = -1.44(1)$ was obtained. (No nonlinearities were observed within uncertainties dominated by the precision of the optical data.) From the intercept and the mass shift of the reference transition (which is a pure $s^2 \rightarrow sp$ transition for which the specific mass shift is small [19,22], one obtains the mass shift in the $A \rightarrow B$ transition. The mass shift between isotopes 164 and 162 is $(2/162/164)M_{A\rightarrow B} = -516(50)$ MHz and is due entirely to specific mass shift. $M_{A\rightarrow B}$ is a mass shift parameter in the notations of [19]. The value of the specific mass shift for the transition $A \rightarrow B$ is typical for transitions where the number of f-electrons decreases by one [23].

The optical isotope shift is known for all stable isotopes

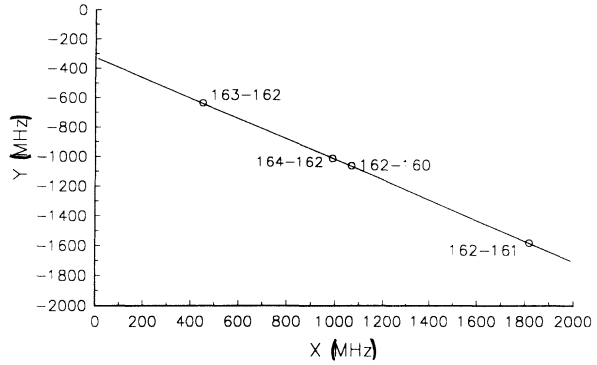

FIG. 6. Modified isotope shifts Y in an optical transition 563.95 nm [19] vs modified isotope shifts in the rf transitions observed in the present work. Typical uncertainties: in Y—3 MHz, in X—0.03 MHz.

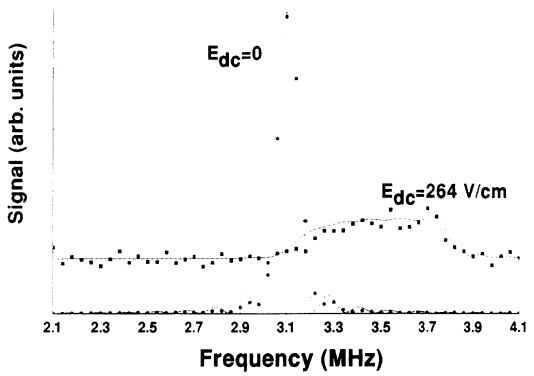

FIG. 7. Experimental line shapes of an rf transition without dc electric field (solid circles) and with a dc electric-field parallel to the rf electric field (squares). Averaging—20 pulses per point. Solid lines—fitting curves generated by numerical integration of the Schrödinger equation (see text). Free parameters of the fit are overall scale and background (common for both curves) and the reduced matrix element.

including 158 and 156. Thus under the assumption of linearity of the King plot, it is possible to determine (with a limited accuracy) the rf isotope shifts and energy separations W_B-W_A for these isotopes, even though their transitions were not observed. The corresponding values are given in the second column of Table II.

The deduced values of hyperfine constants for the odd isotopes are given in the last 5 columns of Table II. For isotope 161, the observed rf frequencies could be well described by magnetic dipole and electric quadrupole hfs. However, in order to obtain an adequate fit for isotope 163, it was necessary to introduce an effective magnetic octupole interaction. The fit was sensitive only to c_B-c_A, not the individual magnetic-octupole constants. As discussed in detail, e.g., in [24], the apparent magnetic-octupole hfs does not necessarily arise from a nuclear magnetic-octupole moment, but may be caused by second-order magnetic-dipole and electric-quadrupole interactions that mix a given state with other states of the same parity.

VII. MEASUREMENT OF ELECTRIC POLARIZABILITY

Two different methods were used to determine the electric polarizability of states A and B. In one of them [11], the positions and line shapes of the lowest-frequency rf transitions (3.10 MHz: $F_A=10.5\rightarrow F_B=10.5$, isotope 163; and 68.83 MHz: $F_A=7.5\rightarrow F_B=7.5$, isotope 161) were studied when a dc electric field was applied between the field plates simultaneously with the rf field. An example of an rf line shape in the presence of a dc electric field is given in Fig. 7. Qualitatively, a dc electric-field results in appearance of a radio frequency-independent background due to quantum oscillations between A and B caused by the Stark mixing, and also in changes in resonance frequency which are different for components with different $|m_F|$. Due to the extreme proximity of the states between which the rf transition occurs, one expects the polarizability to be dominated by Stark mixing between these states, rather than their mixing with other states which are over 200 cm^{-1} away. In this case, in the limit of small dc fields, the Stark shift of the 3.10-MHz transition should be roughly 20 times larger than that of the 68.83-MHz resonance. This was indeed observed experimentally. Therefore, the polarizability can be expressed in terms of a single reduced $E1$ matrix element[4] $\langle B,J\|D\|A,J\rangle$. The numerical value of this parameter was extracted by fitting experimental data to theoretical line shapes (see Fig. 7). These line shapes were generated as sums of contributions from each Zeeman component computed by numerical integration of the Schrödinger equation and averaging over the rf phase.

The original measurements reported in [11] were carried out with the population scheme of the state A involving the transitions GC, CA [Fig. 3(a)]. In these measurements the following value of the reduced dipole moment was obtained: $|\langle B,J\|D\|A,J\rangle|=1.1(2)\times10^{-2}ea_0$, where e is electron charge and a_0 is the Bohr radius. However, it was noticed that the UV light exciting the GC transition was also causing significant photoionization. The resulting space-charge effects could, in principle, alter the average electric field on the atoms and introduce systematics. Therefore, the polarizability measurements were repeated with the Gb, bA population scheme in which no noticeable photoionization occurred. In the new measurements, the dc electric field was 0–300 V/cm

[4]For a definition and discussion of reduced matrix elements, see, e.g., [25]. A matrix element between components of A and B corresponding to the same F and m_F can be written as

$$\langle B,F,m_F|\mathbf{D}|A,F,m_F\rangle=\sum_{m_J}\frac{m_J\langle B,J\|D\|A,J\rangle}{\sqrt{J(J+1)(2J+1)}}\times\langle J,m_J,I,m_F-m_J|F,m_F\rangle^2,$$

where $\langle J,m_J,I,m_F-m_J|F,m_F\rangle$ is a Clebsch-Gordan coefficient.

in the case of the 3.10-MHz transition and up to 2000 V/cm for the 68.83-MHz transition. The following value of the reduced dipole moment was obtained: $|\langle B,J\|D\|A,J\rangle|=1.5(1)\times10^{-2}ea_0$.

The electric-dipole matrix element between the states A and B was also measured with a level-crossing technique involving no rf electric field. Consider the $F=10.5$ components of the states A and B for the isotope 163 which are separated by 3.10 MHz in the absence of external fields. Since these states have different Lande factors g_F, by applying magnetic field $\mathbf{B}=B\hat{\mathbf{z}}$ their Zeeman sublevels with the same m_F can be brought to a crossing. In the presence of an electric field $\mathbf{E}=E\hat{\mathbf{z}}$, the Stark mixing for a nearly-crossed pair of sublevels is enhanced due to the small energy separation. If, as above, A is populated at $t=0$ and B is probed at a later time, one can observe quantum oscillations of population between the two states. The amplitude and frequency of these oscillations in general depend on the dipole moment matrix element.

The dependence of the signal on the magnetic field with fixed time delay 8 μsec between population and probe pulses and fixed values of electric field at 5,10, 15, and 20 V/cm are shown in Fig. 8. With the weakest electric field (5 V/cm), the peak positions correspond to the crossings of the $m_F=-10.5$, -9.5, -8.5, etc., at the corresponding magnetic-field values 1.46, 1.62, 1.81 G, etc. The amplitudes of the peaks are proportional to the populations of the corresponding m_F sublevels of A at $t=+0$ and the squares of the appropriate Clebsch-Gordan coefficients. Apart from the overall size, the shape of the magnetic-field dependence of the signal with the weakest electric fields is insensitive to the value of the dipole matrix element and is used to determine relative populations of the Zeeman components. These populations may not be exactly equal due to incomplete saturation of the population transitions[5]. At higher electric fields, several Stark-induced oscillations between A and B occur in the time between population and probing. The resulting complicated shape of the signal as a function of magnetic field sensitively depends on the dipole matrix element. From the fits shown in Fig. 8, one again obtains the value $|\langle B,J\|D\|A,J\rangle|=1.5(1)\times10^{-2}ea_0$. Both in this case and in the rf resonance Stark-shift measurements, the errors are, to a large extent, due to the uncertainty in the separation between the electrodes and are not entirely independent. One thus arrives at the final value of the matrix element: $|\langle B,J\|D\|A,J\rangle|=1.5(1)\times10^{-2}ea_0$. A corresponding z projection of the dipole moment is

$$\langle B,J,m_J|\mathbf{D}|A,J,m_J\rangle=\frac{m_J}{\sqrt{J(J+1)(2J+1)}}\times\langle B,J\|D\|A,J\rangle\ ;$$

its maximum value is $3.1(2)\times10^{-3}ea_0$ with $|m_J|=J$.

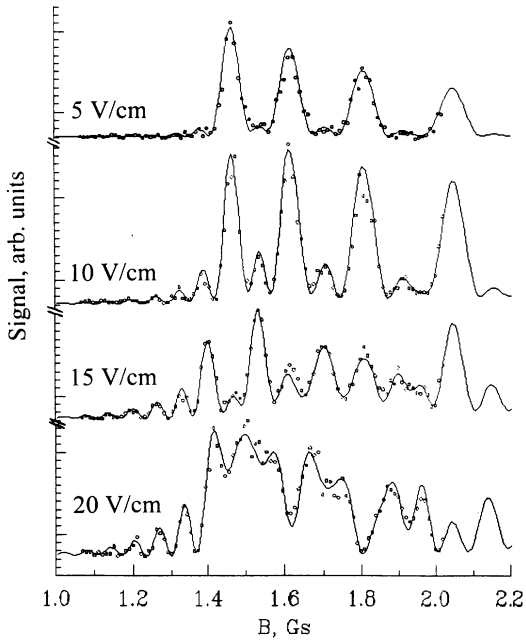

FIG. 8. Level-crossing signals for several extreme Zeeman sublevels ($m_F=-10.5,-9.5$, etc.) of the $F=10.5$ components of the states A and B with dc electric field $\mathbf{E}\|\mathbf{B}$, $E=5$–20 V/cm. Circles: experimental points taken with time delay $t=8$ μsec between population of A and probing of B. Each point represents averaging over 10 pulses. Solid lines—fitting curves (see text).

VIII. PROBE TRANSITION SPECTROSCOPY

Since the probe laser pulses were produced by a narrow-bandwidth dye amplifier (see Sec. II), it was possible to perform spectroscopy on the probe transition [$B\rightarrow D$, Fig. 3(d)] and determine its isotope shift and hyperfine structure. This measurement provided information which was used in identification of the rf $A\rightarrow B$ transitions (Sec. V). In addition, hyperfine constants for the upper state D (37299.36 cm^{-1}, $J=11$) were determined.

A procedure used for the probe transition spectroscopy was similar to that used for rf spectroscopy (Sec. IV) except the probe light frequency was scanned over a range $\sim$10 GHz by scanning the seeding laser, while the frequencies of the pump lasers and the rf field were tuned to resonance and the probe beam was attenuated. In order to calibrate the probe frequency scan, a fraction of the

TABLE III. Hyperfine constants of the level D (37299.36 cm^{-1}, $J=11$) obtained by probe transition spectroscopy.

Isotope	a_D, MHz	b_D, MHz
161	−107(4)	4870(200)
163	150(3)	5080(100)

[5]For the level-crossing measurements, the population scheme Gb,bA [Fig. 3(a)] was used.

TABLE IV. Isotope shifts $W_{BD}(A_2)-W_{BD}(A_1)$ obtained by probe transition spectroscopy.

Isotopes (A_2-A_1)	164-162	163-162	162-161
Isotope shift, MHz	−200(70)	−110(60)	−140(80)

seeding laser output was used to generate transmission fringes of a stabilized Fabry-Perot interferometer with a free spectral range 5 GHz. When the radio frequency is tuned to a resonance corresponding to an even isotope, there is a single resonance in the probe spectrum; when the rf resonance corresponds to an odd isotope and a component of B with total angular momentum F, there are in general three resonances in the probe spectrum corresponding to $\Delta F=+1,0$ and -1. According to the $\Delta F=\Delta J$ rule for relative intensities, the $\Delta F=1$ transitions are the strongest. The $\Delta F=0,-1$ transitions are suppressed compared to them by factors of ~ 50 and ~ 7000, respectively. In fact, the $\Delta F=-1$ transitions were so weak that they were not observed experimentally.

Results on isotope shift and hyperfine structure of level D are collected in Tables III and IV. It should be noted that the isotope shift in the $B\rightarrow D$ transition is relatively small; this, combined with a limited resolution of the optical isotope shift (IS) measurement, precludes its separation into mass and field shifts.

Isotope shifts are extensively used for electron configuration assignments in complex spectra [22]. In dysprosium, corresponding studies in numerous transitions to high-lying levels were carried out in [26]. Among transitions studied in that work there was one involving level D. The authors of [26] were not able to assign a configuration to this level but they suggested that it may belong to a mixed $4f^9 5d6s6p$ configuration. This suggestion is corroborated by the present isotope shift result since, as can be seen from the empirical values of isotope shifts for various configurations given in [21], among the possible configurations in this energy range, it is only $4f^9 5d6s6p$ for which a relatively small isotope shift in a transition from level B ($4f^9 5d^2 6s$) can be expected.

IX. AUXILIARY LIFETIME MEASUREMENTS

In connection with the study of the nearly degenerate opposite parity levels A and B, lifetimes of a number of other excited states were measured. These measurements were part of a search for appropriate population and detection schemes for the levels of interest. Previously [12], we reported lifetime measurements of 27 odd parity levels in the range 35 000–37 000 cm^{-1}. Here we extended these measurements to several other states which include states of both even and odd parity.

For the present lifetime measurements, several schemes were used to populate the state under investigation (Fig. 9). In scheme (a), atoms were excited from the ground state or from the thermally populated state G' by an $E1$ transition. We also used two-photon excitation (b) and stepwise three-step $E1$-$E1$-$E1$ (c) and two-photon–$E1$-$E1$ (d) excitation. In the stepwise excitation schemes, in analogy to what was described in Sec. II, the first two

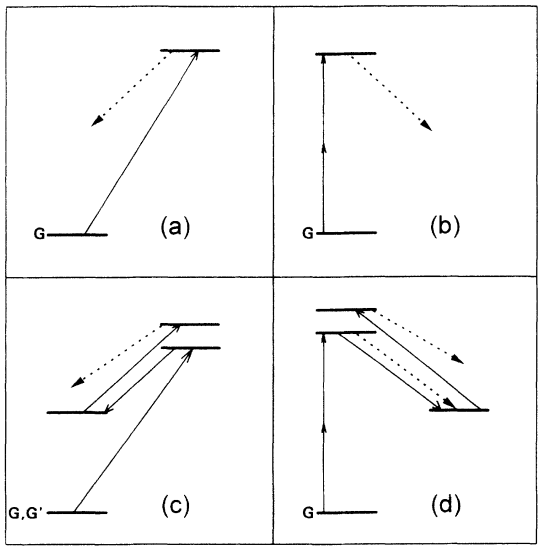

FIG. 9. Excitation schemes for the auxiliary lifetime measurements. Solid lines, laser-induced transitions; dashed lines, fluorescence.

laser pulses transferred a significant fraction of the ground state population to an intermediate metastable level (A, G', or B). The third laser pulse, which followed the first two pulses after a typically 1-μsec delay, excited the state under investigation. In several cases, instead of the second laser-induced transition, atoms spontaneously decayed to an intermediate metastable level (K and the odd parity level 17 513.33 cm^{-1}).

The lifetimes were measured by recording the temporal evolution of fluorescence signals. The output of the photomultiplier was directly connected to a 50-Ω input of a Tektronix 2430A digital oscilloscope used for digitizing, averaging and recording of the fluorescence decay signals. Combinations of colored glass and interference filters were used to select individual decay channels in fluorescence, and thus to suppress scattered light contributions to negligible levels. Entire experimental profiles were fitted with profiles generated as convolutions of photomultiplier response to a short (intentionally scattered) light pulse with exponentials.

A summary of the lifetime measurements (level energies and angular momenta, excitation schemes, detected fluorescence wavelengths and measured lifetimes) is given in Table V. The quoted uncertainty is entirely systematic, and is mainly due to unknown details of the fluorescence evolution on the time scale comparable to the laser-pulse duration. For completeness, lifetime measurement results described in Sec. III are also included in Table V. Results of previous lifetime measurements by other authors for several even parity states are listed in the last column of Table V. They are in agreement with the present measurements.

It should be noted that the $E1$ amplitude of the transition from the ground state to level 36 341.53 cm^{-1} [level C, Figs. 1,3(a)] which appears in Table V is strongly

TABLE V. Auxiliary lifetime measurement summary. The excitation schemes are given according to Fig. 9.

Energy (cm^{-1})	J	Excitation scheme	λ fluor. (nm)	τ, ns this work	τ, ns other Refs.
			Even parity states		
29 706.72	10	*d*	507	101(10)	
30 444.88	7	*b*	437,456	334(20)	
30 475.95	6	*b*	455	190(30)	
30 600.15	8	*b*	453	400(40)	
30 979.53	8	*b*	445	18(10)	
31 124.80	7	*b*	424,449	442(30)	
34 174.66	9	*d*	376	< 16	
34 689.19	9	*d*	441,459	18(10)	
34 776.04	10	*d*	457	148(20)	
35 377.51	8	*b*	360,394,457	20(10)	
35 385.78	10	*b,d*	394,444,457	17(10)	
37 299.36	11	*d*	410	21(10)	
			Odd parity states		
12 892.76	10			> 200 μsec	
17 513.33	10		See Sec. III	> 200 μsec	
17 727.15	9			2220(40)	2150(100) [16] 2700(400) [17]
18 857.04	7	*a,c*	530	1320(150)	1030(70) [17]
21 675.28	7	*a,c*	461	120(10)	121(5) [16] 117(8) [17] 114(9) [34]
21 783.42	7	*a,c*	459	72(6)	75(2) [16] 73(6) [17] 73(6) [34]
21 899.22	8	*a,c*	457	1500(150)	1200(50) [16] 1205(97) [34]
22 061.29	7	*a,c*	453	> 4 μsec	~ 10 μsec[a]
36 341.53	9	*a*	573	70(10)	
36 868.73	10	*c*	567	31(10)	
37 182.98	11	*c*	534	21(10)	

[a]Estimated from the relative oscillator strengths given in [35].

suppressed. Therefore, the branching ratio of the decay to the ground term levels is nearly zero. Since in the conditions of the earlier experiment [12], only fluorescent decay to the ground term was detected, this transition was not observed at that time.

X. IONIZATION SPECTROSCOPY

In the process of choosing an appropriate population scheme for the level A [Fig. 3(a)], laser L_1 was tuned to a UV resonance and the fluorescence from the upper state of this resonance was monitored, while laser L_2 was scanned in the vicinity of an expected stimulated emission resonance. A stimulated emission transition to an even parity state should manifest itself as depletion of the fluorescence signal. If the stimulated emission transition is saturated, one expects ~50% depletion. In practice, however, as laser L_2 was scanned, a large number of depletion resonances were observed with depletion as much as 100%. These resonances were unexpected from the known energy levels of Dy I, and their spectral widths were typically a few cm^{-1}.

Since the sum of photon energies of lasers L_1 and L_2 was greater than the ionization limit 46 900 cm^{-1} [27], a possible explanation of these resonances could be that they correspond to transitions to relatively narrow autoionization states. Such states were observed in other rare-earth elements (see, e.g., [28–32]). In order to check this hypothesis, ions produced in the interaction region were detected simultaneously with fluorescence. This was done by applying a bias to the electrodes, and detecting the resulting ion current with a charge-sensitive amplifier. The signature of a transition to an autoionization state is a peak in the ion signal accompanied by a reduction in fluorescence. This was indeed observed for the unexpected resonances (an example of simultaneous recording of the ion signal and fluorescence is shown in Fig. 10). Therefore, these resonances correspond to transitions to autoionization states.

We have observed autoionization states in the range 52 750–53 250 cm^{-1} using two-step laser excitation from the ground state with the following intermediate states of odd parity: 36 341.53 cm^{-1} ($J=9$), 36 440.19 cm^{-1} ($J=9$), and 36 441.99 cm^{-1} ($J=7$). For a given inter-

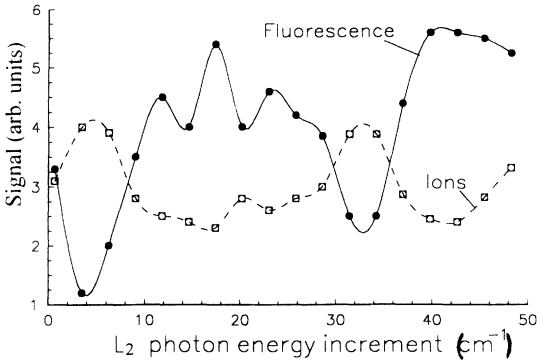

FIG. 10. An example of autoionization resonances. Laser L_1 was tuned to resonance corresponding to a transition $G \rightarrow 36341.53$ cm^{-1}, laser L_2 photon energy was scanned around 16753 cm^{-1}. An autoionization resonance manifests itself as an increase in ion signal accompanied by fluorescence depletion. Experimental points are connected with smooth lines to provide a visual guide.

mediate state, there were typically several autoionization states per a 100 cm^{-1} energy interval.

A systematic study of the observed autoionization states including measurements of energy interval and width distributions could be of interest in connection with the quantum chaos problem and the theory of dynamic enhancement of perturbations [33].

XI. CONCLUSION

We have studied a pair of opposite parity states in atomic dysprosium which are nearly degenerate. Efficient schemes for population and probing of these states involving pulsed laser excitation were realized, and the state lifetimes were measured. The small energy separation between the states allows one to use rf spectroscopy on the transition $A \rightarrow B$. By means of this method, energy intervals between various isotope and hyperfine components were measured. The smallest energy interval (3.1 MHz) is ~ 300 times smaller than the interval between the $2^2s_{1/2}$ and $2^2p_{1/2}$ levels of hydrogen, which are separated only by the Lamb shift (1058 MHz). From an analysis of the energy separations, isotope shift and hyperfine structure of the levels A,B was determined. rf line shapes in the presence of a dc electric field were used to measure electric polarizability. The electric dipole matrix element between states A and B was also measured by analyzing level-crossing signals in the presence of a dc electric field. The results (relatively long lifetimes of both states, the magnitude of polarizability, etc.) indicate that P and P,T violation experiments with this system are promising. Work in this direction is in progress in our laboratory.

In addition, information about various other states of dysprosium was obtained, including data from lifetime, isotope shift and hyperfine-structure measurements and observation of autoionization states.

ACKNOWLEDGMENTS

The authors are grateful to I. B. Khriplovich, M. G. Kozlov, R. Marrus, and J.-F. Wyart for useful discussions, to E. Gluskin, R. Falcone, W. Knight, V. Kresin, J. Orenstein, H. Shugart, and L. Wald for their technical advice and support, and to R. P. Aditya, P. Miller, and V. Yepishin for technical assistance. This research has been supported by National Science Foundation Grant No. PHY-9111771.

[1] D. N. Stacey, in *Atomic Physics 13,* edited by H. Walther, T. W. Hansch, and B. Neizert (AIP, New York, 1993), p. 46.
[2] E. D. Commins, Phys. Scr. **T46**, 92 (1993).
[3] M. A. Bouchiat, in *Atomic Physics 12,* edited by J. C. Zorn and R. R. Lewis (AIP, New York, 1991), p. 399.
[4] L. R. Hunter, in *Atomic Physics 12* (Ref. [3]), p. 429.
[5] J. H. Christenson, J. W. Cronin, V. L. Fitch, and R. Turlay, Phys. Rev. Lett. **13**, 138 (1964).
[6] I. B. Khriplovich, *Parity Non Conservation in Atomic Phenomena* (Gordon and Breach, Philadelphia, 1991).
[7] W. C. Martin, R. Zalubas, and L. Hagan, *Atomic Energy Levels—The Rare Earth Elements* (National Bureau of Standards, Washington, DC, 1978).
[8] V. A. Dzuba, V. V. Flambaum, and I. B. Khriplovich, Z. Phys. D **1**, 243 (1986).
[9] M. A. Bouchiat and C. Bouchiat, J. Phys. (Paris) **35**, 899 (1974); **36**, 483 (1975).
[10] M. G. Kozlov, V. A. Dzuba, and V. V. Flambaum (private communication).
[11] D. Budker, D. DeMille, E. D. Commins, and M. S. Zolotorev, Phys. Rev. Lett. **70**, 3019 (1993).
[12] D. Budker, E. D. Commins, D. DeMille, and M. S. Zolotorev, Opt. Lett. **16**, 1514 (1991).
[13] P. Drell and S. Chu, Opt. Commun. **28**, 343 (1979).
[14] N. F. Ramsey, *Molecular Beams* (Oxford, New York, 1990).
[15] W. H. Press, B. P. Flannery, S. A. Teukolsky, and W. T. Vetterling, *Numerical Recipes. The Art of Scientific Computing* (Cambridge University Press, New York, 1986).
[16] M. Gustavsson, H. Lundberg, L. Nilsson, and S. Svanberg, J. Opt. Soc. Am. **69**, 984 (1979).
[17] V. N. Gorshkov, V. A. Komarovskii, A. L. Oserovich, N. P. Penkin, and R. Khefferlin, Opt. Spektrosk. **48**, 657 (1980) [Opt. Spectrosc. (USSR) **48**, 362 (1980)].
[18] W. J. Childs, Phys. Rev. A **2**, 1692 (1970).
[19] G. J. Zaal, W. Hogervorst, E. R. Eliel, K. A. H. van Leeuwen, and J. Blok, J. Phys. B **13**, 2185 (1980); E. R. Eliel, W. Hogervorst, G. J. Zaal, K. A. H. van Leeuwen, and J. Blok, *ibid.* **13**, 2185 (1980), p. 2195.
[20] I. I. Sobelman, *Atomic Spectra and Radiative Transitions* (Springer-Verlag, New York, 1992), p. 211.
[21] J.-F. Wyart, Ph.D. thesis, University Paris–Sud, Orsay, 1973; (private communication), 1992.

[22] W. H. King, *Isotope Shifts in Atomic Spectra* (Plenum, New York, 1984).
[23] J. Bauche, J. Phys. (Paris) **35**, 19 (1974).
[24] W. J. Childs, Case Studies Atom. Phys. **3**, 215 (1972).
[25] L. D. Landau and E. M. Lifshitz, *Quantum Mechanics. Non-Relativistic Theory* (Pergamon, New York, 1977), p. 94.
[26] S. A. Ahmad, A. Venugopalan, and G. D. Saksena, Ind. J. Pure Appl. Phys. **19**, 1183 (1981); Spectrochim. Acta Part B **37**, 181 (1982); **38**, 639 (1983).
[27] E. F. Worden, R. W. Solarz, J. A. Paisner, and J. G. Conway, J. Opt. Soc. Am. **68**, 52 (1978).
[28] G. I. Bekov, V. S. Letokhov, O. I. Matveev, and V. I. Mishin, Pis'ma Zh. Eksp. Teor. Fiz. **28**, 308 (1978) [JETP Lett. **5**, 284 (1978)].
[29] P. Camus, A. Debarre, and C. Morillon, J. Phys. B **13**, 1073 (1980).
[30] G. I. Bekov, E. P. Vidolova-Angelova, L. N. Ivanov, V. S. Letokhov, and V. I. Mishin, Zh. Eksp. Teor. Fiz. **80**, 866 (1981) [Sov. Phys. JETP **53**(3), 441 (1981)].
[31] Hu Sufen *et al.*, Chinese Phys. Lett. **6**(2), 64 (1989).
[32] Wu Bi-ru *et al.*, J. Phys. B **25**, 355 (1992).
[33] V. V. Flambaum (private communication).
[34] R. Hotop and J. Marek, Z. Phys. A **287**, 15 (1978).
[35] N. P. Penkin and V. A. Komarovsky, J. Quant. Spectrosc. Radiat. Transfer **16**, 217 (1976).